

Dielectric screening and vacancy formation for large neutral and charged Si_nH_m ($n > 1500$) nanocrystals using *real-space* pseudopotentials

Timothy Liao 

Department of Physics, The University of Texas at Austin, Austin, Texas 78712, USA

Kai-Hsin Liou

McKetta Department of Chemical Engineering, The University of Texas at Austin, Austin, Texas 78712, USA

James R. Chelikowsky *

*Center for Computational Materials, Oden Institute for Computational Engineering and Sciences,
McKetta Department of Chemical Engineering, and Department of Physics,
The University of Texas at Austin, Austin, Texas 78712, USA*



(Received 30 November 2021; accepted 4 May 2022; published 31 May 2022)

A commonly used procedure for computing the properties of defects in crystalline materials is to consider a large supercell that includes the defect of interest. This is a straightforward technique as standard energy band codes can be used for such computations. For neutral defects, the only impediment of such an approach is to avoid defect-defect interactions between adjoining cells. However, this procedure can be complex if the defect of interest is charged as the system at large contains Coulombic divergences. Moreover, some have recently argued that the conventional definition of formation energies for charged defects cannot be reconciled with statistical mechanics. Here, we focus on an alternative approach. We consider large nanocrystals wherein a charged defect can be placed. Since the system is confined, a charged defect within the nanocrystal does not result in a Coulombic divergence. The chief impediment is computational, i.e., while no defect-defect or Coulombic divergences are present, the nanocrystal must be sufficiently large to allow the system to properly replicate a bulklike configuration. With the development of new algorithms and hardware advances, computations for systems of sufficient size to address this issue are feasible. In particular, we solve the Kohn-Sham equation in *real space* using pseudopotential-density-functional theory for large silicon nanocrystals, which contain thousands of atoms. We focus on (i) the screening of a point charge and (ii) the formation of a charged vacancy in hydrogen-terminated silicon nanocrystals. This approach allows us to examine the role of quantum confinement in addition to exploring the bulk limit. Comparisons to other methods confirm the viability of this approach.

DOI: [10.1103/PhysRevMaterials.6.054603](https://doi.org/10.1103/PhysRevMaterials.6.054603)

I. INTRODUCTION

A key aspect of electronic materials is the controlled introduction of defects or dopants to alter intrinsic properties for electronic device applications. The nature of these defects across different length scales is a matter of continued study as the length scales in device applications approach the nanoregime. In particular, the interplay of restricted dimensionality and quantum confinement can complicate the role defects play in altering electronic properties, e.g., well-known rules for describing defects in the bulk may become inoperative at the nanoscale [1].

Here, we illustrate how computational methods based on confined systems in *real space* can be used to predict the emergence of nanoscale electronic properties in semiconductors such as dielectric screening and how these properties evolve from the nanoscale to the bulk limit.

Silicon nanocrystals (NCs) often serve as a prototypical semiconductor owing to the large number of theoretical

and experimental studies [2]. The possible application of Si NCs as photovoltaic and luminescent devices is among the forefront of silicon research [3–10]. Here, we examine the approaches for the modeling of *charged* systems with Si NCs to avoid issues with divergent Coulomb terms. Traditionally, using confined systems to model defects, charged or not, in the bulk limit has been problematic as one needs to consider very large systems to converge a solution [11]. However, the advent of computational methods in *real space* allows one to consider systems with thousands of atoms [12–14]. The use of confined systems offers an additional advantage. We can examine the role of quantum confinement on the electronic properties of defects and the emergence of bulk configurations as the size of a NC is increased.

Our focus resides in two areas: First, we will compute dielectric properties by considering the screening of a test charge. This will allow us to examine how dielectric properties evolve and assess the distribution of the screening charge. Similar computations have been done for a number of NC configurations, although well before the bulk limit is achieved [15–24]. Computational demands have limited previous calculations of the microscopic dielectric screening function to

*jrc@utexas.edu

using NCs consisting of ~ 700 atoms [25] whereas we will consider systems up to 5500 atoms. We will also avoid *ad hoc* procedures needed to avoid the Coulombic divergence when using supercells containing a charged system [26,27]. Second, we will examine the electronic structure of charged defects. In particular, we examine charged vacancies in bulk silicon. Vacancies are known to lower device performance because they act as carrier traps, i.e., vacancies introduce states in the gap thus decrease the carriers available. The key quantity which determines the vacancy concentration [28–32] is the formation energy [33–57].

A popular method of modeling a vacancy centers on considering a supercell of the bulk material wherein the system retains translational symmetry. If the cell is of sufficient size, the vacancy in each cell will not interact with vacancies in adjoining cells. To remove vacancy-vacancy interactions requires large cells.

When the vacancy considered is charged, special care is required to resolve the Coulombic divergence [53,56,58–61]. Also, some workers have argued that the conventional definition of formation energy used for supercells cannot be reconciled with statistical mechanics [31].

As an example, consider a positively charged vacancy. One procedure to avoid charging the supercell is to add a compensating background charge to keep the cell neutral. The consequences of adding this background, e.g., determining the total energy of the vacancy, can be problematic. A recently proposed alternative is to place the “removed” electron into an empty state in which case the system remains neutral [31]. One might argue that the added electron reflects a situation where the system resembles an “excited state.” Nonetheless, the agreement with other computational approaches appears to be satisfactory.

In the case of a NC charging issues are moot, the electron is removed from the system, and no divergent terms exist. Of course, we can also examine the case where the electron is not removed from the NC and assess what differences might exist. We can also examine such issues as a function of NC size to assess how the charged vacancies converge to the bulk limit. We compare our structures and formation energies to previous work and assess how large NCs need be to reproduce the bulk limit.

II. COMPUTATIONAL METHODS

We form our Si NCs by taking a spherical fragment from a bulk crystal with a calculated lattice constant of 5.37 \AA , about 1% smaller than the experimental value. At the surface of the NC, broken Si bonds are passivated with hydrogenlike atoms. The role of the passivating atoms is solely to remove any dangling bond states from the gap and to structurally terminate the NC. Singly coordinated Si surface atoms are removed and replaced by the passivating H-like atoms. The radius of the NC is defined as the distance from the center of the NC to the furthest passivating atom. A ball and stick model of a large NC is illustrated in Fig. 1.

We solve the Kohn-Sham equation [63,64] on a uniform grid in *real space* as implemented in the PARSEC code [12,65–67]. The Laplacian in the kinetic-energy term is expanded using high-order finite differencing. Periodic and confined

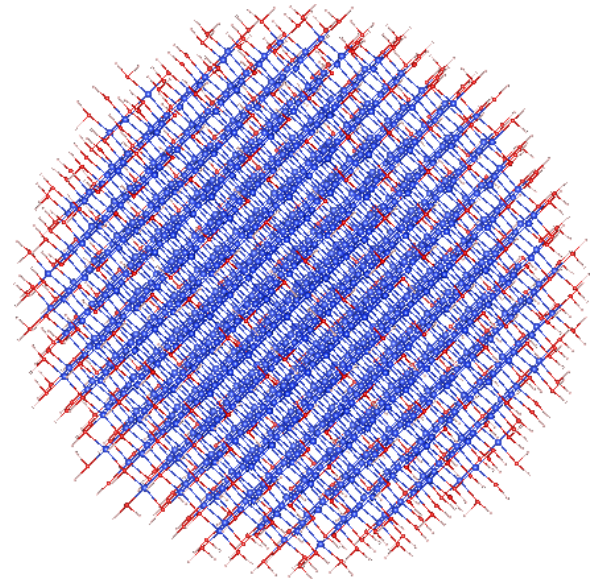


FIG. 1. Ball and stick model [62] of a Si nanocrystal, $\text{Si}_{1523}\text{H}_{524}$, of radius 39 a.u. (1 a.u. = 0.5292 \AA). The boundary of the bulk-terminated fragment is passivated by H-like atoms (light pink). When structural optimization is performed, the Si atoms at the surface (red) are not relaxed, whereas the interior Si (blue) atoms are.

boundary conditions are available in this code. For NCs, we use confined boundary conditions. We enclose the NC in a spherical domain to simulate an isolated NC as the wave functions are required to vanish beyond the domain boundary. The domain boundary is set to be at least 7 a.u. (atomic units) from the outermost atom of the NC. This ensures that the electronic structure of the NC will not be affected by the domain size.

The local density approximation (LDA) as determined by Ceperley and Alder [68] and parametrized by Perdew and Zunger [69] is used for the exchange-correlation functional within density-functional theory (DFT). Troullier-Martins pseudopotentials [70] are used with Si having a valence configuration $3s^2 3p^2 3d^0$ and a cutoff radius of 2.49 a.u. for all the angular momentum channels. The H-like pseudopotential has a valence $1s^1$ using a 1.99 a.u. cutoff. The large radius for the H-like atom allows a “soft” pseudopotential, but preserves the bond length of the Si-H bond and yields a reasonable description of a H-H bond and the Si-H charge density. The P and Al pseudopotentials were constructed using valence configurations $3s^2 3p^3 3d^0$ and $3s^2 3p^1 3d^0$, respectively. The cutoff radii for the angular momentum channels for P and Al are 1.95 and 1.98 a.u., respectively. We employ spin polarization to describe the electronic structure of defects. In all cases, we use a uniform grid spacing h . The spectral features are typically well converged with $h = 0.7$ a.u., which we use to study the dielectric screening. For accurate structural relaxation problems such as that of the vacancy, we use a grid of $h = 0.5$ a.u. All atoms are relaxed [71–73], save the surface atoms. This distinction is indicated in Fig. 1. Upon relaxation, the residual forces are required to be less than $\sim 10^{-3} \text{ Ry/a.u.}$

A key aspect of our work is the availability of algorithms that can address large systems. The “routinely solvable” system size for materials has increased from dozens of atoms in

the 1990s to thousands of atoms today, owing to algorithm developments and advances in computing power. *Real-space* pseudopotential-DFT coupled with a Chebyshev-filtered subspace iteration algorithm (CheFSI) can be used to solve the electronic structures of systems containing over 26000 atoms [14]. Reducing the computational load for solving the Kohn-Sham equation rests on an efficient eigensolver, which can be accomplished with subspace filtering. During a self-consistent-field (SCF) calculation, the linear eigenvalue problems do not need to be solved to full accuracy in the initial iterations when the electronic charge density is far from converged [74]. CheFSI exploits this characteristic of SCF calculations and focuses on improving the wave functions and electronic charge density at the same time during the SCF cycle. This strategy proves quite efficacious when solving the nonlinear eigenvalue problem defined by the Kohn-Sham equation.

CheFSI can be used to approximate the invariant subspace associated with the occupied states in a *real-space* DFT calculation algorithm. The advantages of using Chebyshev polynomial filtering are as follows: (1) It only requires multiplying the Hamiltonian matrix with vectors. (2) The three-term recurrence of the Chebyshev polynomials makes the filtering process efficient in terms of a memory footprint. (3) Ritz vectors from a previous SCF iteration can be used as the starting guess for the desired eigenvectors in the current SCF iteration. (4) CheFSI is a block method that increases concurrency and memory efficiency.

The key operation in CheFSI is the repeated application of the Hamiltonian \mathcal{H} , expressed as a “damped” Chebyshev polynomial of degree m , $P_m(\mathcal{H})$, on an initial subspace $\{\psi_i\}$ at each SCF step. The new basis is

$$\{\hat{\psi}_i\} = P_m(\mathcal{H})\{\psi_i\}. \quad (1)$$

If the polynomial is properly constructed, only components in the desired subspace are preserved. Choosing the proper subspace for the system of interest is in general straightforward. CheFSI is easily five to ten times faster than solving the eigenproblem at each SCF step. Additional details can be found elsewhere [14,74].

III. DIELECTRIC PROPERTIES OF Si NANOCRYSTALS

To approximate the dielectric properties of Si NCs, we place a point charge within the NC. In particular, we replace a Si ionic core potential by either an Al or a P ion core, depending on whether we wish to remove or add a positive charge from the ion core, respectively. We keep the number of electrons constant.

The change in the electrostatic (i.e., Hartree) potential due to the rearrangement of the electron density in the presence of the point charge is the difference between the total screened electrostatic potential and the bare point charge potential [25],

$$\delta V_H = \frac{q}{\bar{\epsilon} \cdot r} - \frac{q}{r}. \quad (2)$$

The screening function is given by

$$\bar{\epsilon}(\vec{r}) = \frac{1}{1 + |\vec{r}| \cdot \delta V_H(\vec{r})/q}, \quad (3)$$

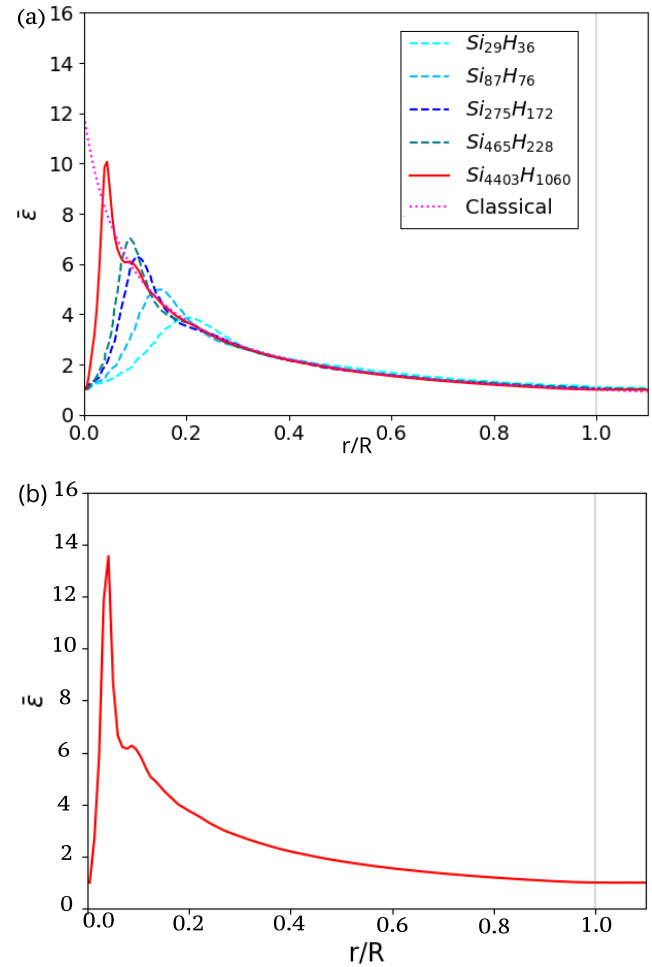


FIG. 2. Spherically averaged screening function vs normalized distance from center. (a) For the screening of a negative charge, we compare results for Si₄₄₀₃H₁₀₆₀ to previous work [25] and to a classical model. (b) The screening of a positive charge.

where $q = \mp 1$, $\delta V_H(\vec{r}) = V_H^0(\vec{r}) - V_H^{-/+}(\vec{r})$, and $V_H(\vec{r})$ is the Hartree potential of the intrinsic (superscript 0) or charged (superscript $-/+$) NC.

In Fig. 2(a), we compare our work for negative screening to a classical model [75],

$$\epsilon_{\text{eff}}(r) = \frac{\epsilon_{\text{classical}}}{1 + \frac{r}{R} \cdot (\epsilon_{\text{classical}} - 1)} \quad (r < R), \quad (4)$$

where R is the NC radius and we take $\epsilon_{\text{classical}} = 11.9$. We also compare to previous work. Results for NCs smaller than and including Si₄₆₅H₂₂₈ are from previous work [25]. Our results for Si₂₇₅H₁₇₂ are indistinguishable to those presented elsewhere [25]. We focus on results for a much larger NC: Si₄₄₀₃H₁₀₆₀.

As the NC size increases, the peak of the screening functions of the NCs moves to smaller distances while the height of the peak increases. The NC screening functions approach the classical model in the range $0 < r \lesssim 0.4R$ with increasing NC size. The long-range tail of the screening function for different sized NCs converges to the classical model. The $\bar{\epsilon}(\vec{r})$ for Si₄₄₀₃H₁₀₆₀ agrees with the trend from the smaller NCs using a plane-wave code [25]. The screening of a positive

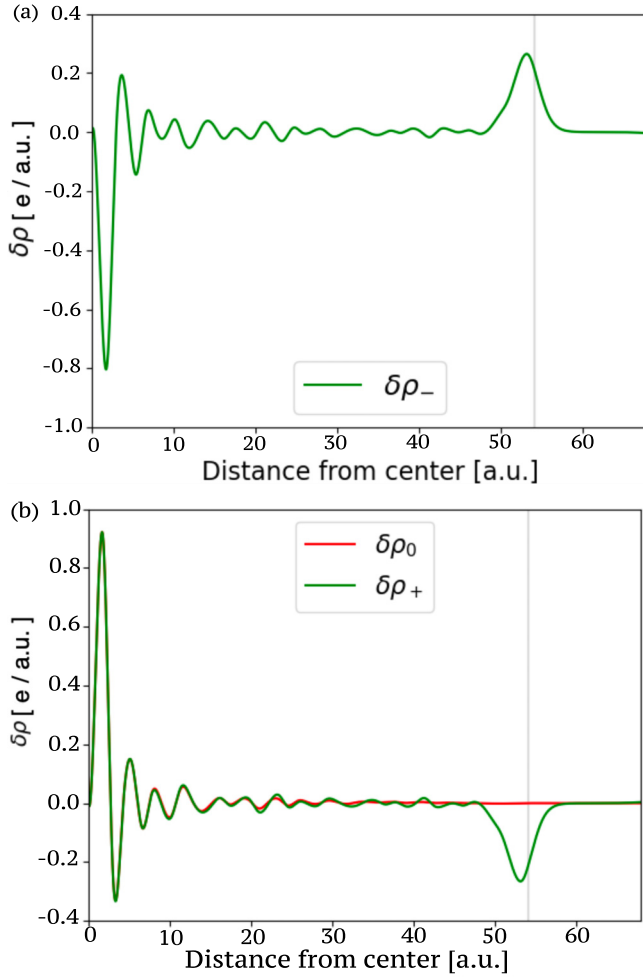


FIG. 3. Spherically averaged change in electron density. The y axes are in units of $e/a.u.$, e being the fundamental charge. Please refer to the text for the definition for the symbols in the legends. The NC surface is at ~ 54.2 a.u., indicated by the gray vertical line. Shown for (a) a negative charge and (b) a positive charge.

charge is shown in Fig. 2(b). The peak in Fig. 2(b) is higher than the peak for $\text{Si}_{4403}\text{H}_{1060}$ in Fig. 2(a). Previous work also found that the peak for the positive-charge screening function is higher than the negative-charge screening function [25].

The induced charge $\delta\rho(\vec{r})$ in $\text{Si}_{4403}\text{H}_{1060}$ for the screening of a point charge is shown in Fig. 3: $\delta\rho_-(\vec{r}) = \rho$ (Al ion replacing the Si ion at the NC center) $-\rho$ (the intrinsic NC), $\delta\rho_+(\vec{r}) = \rho$ (P ion replacing the Si ion at the NC center) $-\rho$ (the intrinsic NC), and $\delta\rho_0(\vec{r}) = \rho$ (P ion replacing the Si ion at the NC center then adding an electron) $-\rho$ (the intrinsic NC). Note that $\int_{\text{all space}} \delta\rho_{+/-}(\vec{r}) \cdot d\vec{r} = 0$ as the total number of electrons did not change, while $\int_{\text{all space}} \delta\rho_0(\vec{r}) \cdot d\vec{r} = 1$ owing to the added electron.

The difference between $\delta\rho_+(\vec{r})$ and $\delta\rho_0(\vec{r})$ is consistent with classical electrostatics [25]. As indicated in Fig. 3(b), an electron added to a NC with a positive point charge at its center will effectively spread itself over the surface. That is, the added electron accommodates the charge deficiency near 54 a.u.

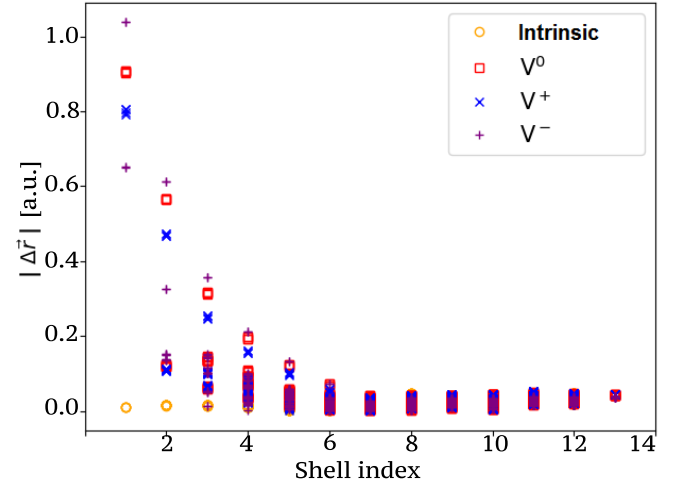


FIG. 4. Atomic relaxation magnitudes in $\text{Si}_{1522}\text{H}_{524}$ (i.e., with vacancy) and in $\text{Si}_{1523}\text{H}_{524}$ (intrinsic).

The largest NC we examined converged to the bulk limit as expected. Accessing NC of this size should allow us to examine defects in NC that from small systems where quantum confinement plays a large role to the bulk limit where it does not.

IV. VACANCY FORMATION ENERGIES

We consider monovacancies in Si NCs, where the vacancy is placed at the center of a NC. By adding a net charge to the system, we can charge the vacancy.

The formation energy of the vacancy [52] is determined by

$$E^{\text{form}} = E_q^{N-1} - E^N + \mu_{\text{Si}} + q(\epsilon_{\text{vbe}} + E_{\text{F}}), \quad (5)$$

where E^N is the total energy of the neutral intrinsic NC, E_q^{N-1} is the total energy of the NC containing a vacancy with net charge $q = 0, \pm 1$, ϵ_{vbe} is the valence band edge eigenvalue of the intrinsic NC of the same size, μ_{Si} is the chemical potential of bulk Si [76], and E_{F} is the Fermi level, which is set to zero.

We consider a set of NCs that range from 29 to 1523 Si atoms: $\text{Si}_{29}\text{H}_{36}$, $\text{Si}_{87}\text{H}_{76}$, $\text{Si}_{275}\text{H}_{172}$, $\text{Si}_{657}\text{H}_{300}$, and $\text{Si}_{1523}\text{H}_{524}$. The sizes of the NCs included have $R = 10.94, 15.98, 22.23, 29.79,$ and 38.63 a.u., respectively.

Atomic relaxation is not significant (< 0.1 a.u.) for shells more than five bonds away from the center of the NC as determined for $\text{Si}_{1522}\text{H}_{524}$ (Fig. 4). Using the elastic constant of Si NCs, the strain energy from the displacements in the outermost three shells is estimated to be about 0.2 meV/atom [77]. As such, there is no residual strain energy of any consequence. Previous work found that when the NC included 12 shells, 95% of the charge density associated with the vacancy lies in the bulk region, indicating a relatively small defect-surface interaction [78].

We found an inward relaxation of the first shell atoms for $V^+/V^0/V^-$ for all the NCs considered, save the smallest NC for V^+ . In Table I, we present fractional distances (relative to the bulk distance $\frac{\sqrt{2}}{2} \cdot \text{lattice constant}$) between the four first shell atoms surrounding the vacancy and their multiplicities in parentheses. The multiplicities are not always six because

TABLE I. Charged and neutral vacancy formation energies (in eV), neighboring distances, and point groups. E^f labels the formation energy. The fractional distance relative to the bulk structure is labeled by fd. The point group symmetry is given by pg. Calculations are shown for several density functionals, included LDA, GGA, and the revised Heyd-Scuseria-Ernzerhof screened hybrid functional (HSE06). In addition to the NC's work, supercell computations are also presented along with the numbers of atoms in the cell. See text for more details.

	V^+			V^0			V^-		
	E^f	fd	pg	E^f	fd	pg	E^f	fd	pg
LDA									
Si ₂₈ H ₃₆	5.21	1.02 (6)	T_d	5.25	0.98 (6)	T_d	8.08	0.96 (6)	T_d
Si ₈₆ H ₇₆	4.39	1.00 (4)	D_{2d}	4.41	0.94 (4)	D_{2d}	6.52	0.92 (6)	T_d
		0.97 (2)			0.85 (2)				
Si ₂₇₄ H ₁₇₂	4.02	0.95 (4)	D_{2d}	3.79	0.90 (4)	D_{2d}	5.42	0.88 (4)	C_{2v}
		0.91 (2)			0.77 (2)			0.83 (1)	
								0.72 (1)	
Si ₆₅₆ H ₃₀₀	3.85	0.90 (4)	D_{2d}	3.58	0.89 (4)	D_{2d}	4.91	0.87 (4)	C_{2v}
		0.83 (1)			0.76 (2)			0.83 (1)	
		0.82 (1)						0.71 (1)	
Si ₁₅₂₂ H ₅₂₄	3.67	0.89 (2)	D_{2d}	3.43	0.89 (4)	D_{2d}	4.57	0.86 (4)	C_{2v}
		0.88 (2)			0.75 (2)			0.83 (1)	
		0.78 (2)						0.71 (1)	
215 atoms [53]	3.20		$\sim D_{2d}$	3.27		D_{2d}	3.88		$\sim D_{3d}$
999 V^+ , 255 V^0 , V^- atoms [51]	3.50		D_{2d}	3.55		D_{2d}	3.71		$\sim C_{2v}$
999 atoms [52]	3.19	0.89 (4)	D_{2d}	3.47	0.89 (4)	D_{2d}	4.23	0.91 (3)	D_{3d}
		0.76 (2)			0.75 (2)			0.69 (3)	
GGA									
Si ₆₅₆ H ₃₀₀	4.02		D_{2d}	3.89		D_{2d}	5.16		C_{2v}
Si ₁₅₂₂ H ₅₂₄	4.04		D_{2d}	3.86		D_{2d}	4.89		C_{2v}
215 atoms [55]	3.61		$\sim D_{2d}$	3.67		D_{2d}	4.04		C_{2v}
511 atoms [31]	~ 3.5			~ 3.6			~ 4.2		
511 atoms [54]	3.49		D_{2d}	3.53		D_{2d}	4.14		D_2
999 atoms [52]	3.50	0.92 (4)	D_{2d}	3.62	0.91 (4)	D_{2d}	4.25	0.89 (4)	C_{2v}
		0.81 (2)			0.78 (2)			0.84 (1)	
								0.73 (1)	
1727 atoms [44]				3.46					
HSE06									
511 atoms [54]	4.06			4.08			5.13		
Experiment [33,84]			D_{2d}	3.6 ± 0.2					C_{2v}

Jahn-Teller induced distortions can break the symmetry. The displacement of the first two shells in Si₁₅₂₂H₅₂₄ are presented in Fig. 5 [62]. Previous work also found an inward relaxation, especially for large NCs [45,46,52,53,57,79–83].

The degeneracy and occupancy of the states introduced into the bulk gap is related to the point group of the relaxed structure. The Kohn-Sham gap states and the point groups are consistent with the tight-binding seminal work by Watkins [51,84]. For V^+/V^0 , there is a half/fully occupied b_2 (representation) state and an empty, doubly degenerate, e state. The b_2 and e states arise from a triply degenerate t_2 state owing to a Jahn-Teller distortion, which lowers the symmetry from that of the perfect crystal (T_d) to D_{2d} [85]. For V^- , the Jahn-Teller distortion lowers the symmetry to C_{2v} and splits the e level. We found the degeneracy and the occupancy number of the gap states to be consistent with the Watkins model (Fig. 6) and with previous work on V^0 [42,43] and on $V^+/V^0/V^-$ [79]. Quantum confinement is responsible for the increase of the Kohn-Sham gap from 1.02 to 1.92 eV upon decreasing the NC size from Si₁₅₂₂H₅₂₄ to Si₂₈H₃₆. The correct degeneracy and occupancy of the gap states are seen in NCs larger than and

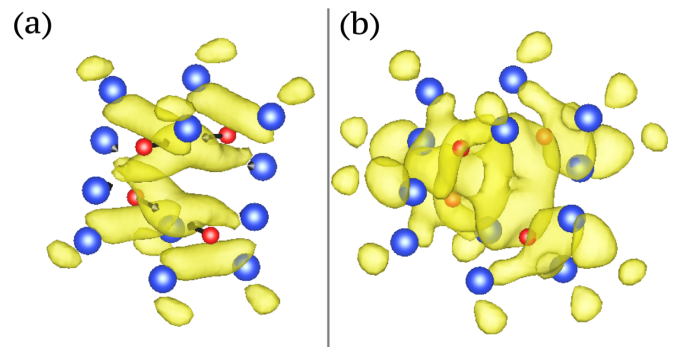


FIG. 5. Wave function squared using an isosurface (yellow) of value $5 \times 10^{-5} e/\text{\AA}^3$, for the (a) filled and (b) empty gap state of the neutral Si₁₅₂₂H₅₂₄. The first (red) and second (blue) shell atoms are shown in their unrelaxed positions. Their relaxation movement vectors, scaled by a factor of 2.5, are represented by the arrows in (a). For the second shell atoms, only a few vectors are (barely) visible. The wave function in (b) is an average over doubly degenerate states.

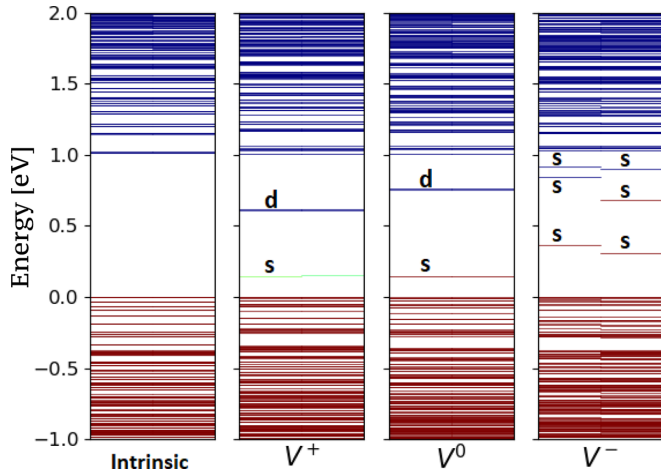


FIG. 6. Kohn-Sham energy levels in the gap for $\text{Si}_{1522}\text{H}_{524}$. We show the gap of $\text{Si}_{1523}\text{H}_{524}$ at the left column for easy comparison. Red, light green, and dark blue denote full, half, and empty occupancy, respectively. The left and right half of each column are for the spin-up and spin-down channels, respectively. Singly (*s*) and doubly (*d*) degenerate states are also labeled.

including $\text{Si}_{86}\text{H}_{76}$ for V^+/V^0 and larger than and including $\text{Si}_{274}\text{H}_{172}$ for V^- .

The point group $D_{2d}/D_{2d}/C_{2v}$ for $V^+/V^0/V^-$ in NCs larger than $\text{Si}_{86}\text{H}_{76}/\text{Si}_{86}\text{H}_{76}/\text{Si}_{274}\text{H}_{172}$ is consistent with the Watkins model and with electron paramagnetic resonance (EPR) studies (for V^+/V^-) [84]. The point groups are presented in Table I in Schoenflies notation.

The symmetry is determined using the distribution of fractional distances among the first shell atoms. Symmetry detection using the entire NC could be erroneous as the boundary atoms are fixed in their bulk positions. Previous theoretical work also found D_{2d} for V^+ [51–55,57,79] and V^0 [42–44,48,51–55,57,79] and C_{2v} for V^- [51,55,79,82]. The lack of Jahn-Teller symmetry breaking in our $\text{Si}_{28}\text{H}_{36}$ stems from the fact that we only relaxed the first shell. We found higher-energy (“metastable”) structures with the D_2 point group for V^- using $\text{Si}_{86}\text{H}_{76}$ and $\text{Si}_{274}\text{H}_{172}$. We suggest that the structures with the D_2 point group for V^- reported in Refs. [54,57] may not represent the ground state.

We examine the defect charge densities in $\text{Si}_{1522}\text{H}_{524}$ which are shown in Fig. 5. The densities are consistent with the Watkins model and the previous work on a smaller NC ($\text{Si}_{166}\text{H}_{124}$) [78]. The density for the filled b_2 state is large between the first shell paired atoms and has a node in the vacancy plane. The dangling bond orbitals of each pair linearly combine as a bonding state. The two bonding states then form an antibonding state, giving rise to the center node. For the empty e state, the dangling bond orbitals of each pair combine to form an antibonding state. Then the two antibonding states form an antibonding state. Thus there are nodes between the paired atoms and at the center.

The formation energy, 3.43 eV, for V^0 using $\text{Si}_{1522}\text{H}_{524}$ agrees with the 3.6 ± 0.2 eV from positron-lifetime experiments [33] (Table I). In Table I, we give results for the formation energy from NC and supercell models for different energy functionals and different sized systems.

We employed two functionals: LDA [69] (mentioned earlier) and the generalized gradient approximation (GGA) as parametrized by Perdew, Burke, and Ernzerhof (PBE) [86,87]. We compared our LDA work with GGA from our work and results from similar-sized systems in the literature [31,44,52]. For our largest system $\text{Si}_{1522}\text{H}_{524}$ the GGA formation energy is 4.04/3.86/4.89 eV for $V^+/V^0/V^-$, respectively, which is 0.37/0.43/0.32 eV higher than the LDA results. This uniform shift agrees quite well with previous comparisons between GGA and LDA for smaller systems [53,55]. Also presented in Table I are results in the literature using a hybrid functional. These results agree quite well (within ~ 0.1 eV) with our GGA computations.

We can also compare our work with an approximate statistical model [31] where the occupancy of the Kohn-Sham levels is constrained. For example, for a positively charged vacancy an electron is placed in an empty state corresponding to the conduction band as opposed to removing the electron from the bulk crystal. As noted, the later process presents computational issues for supercell models where compensating backgrounds are often employed. The approximate statistical model using GGA for a 511-atom supercell yields 3.5, 3.6, and 4.2 eV for $V^+/V^0/V^-$, respectively. In principle, it should be possible to consider an approximate statistical model for a large NC. However, estimating the valence and conduction band energies can be problematic owing to quantum confinement. Nonetheless, we find a statistical model yields energies for the $V^+/V^0/V^-$ for our NC ($\text{Si}_{656}\text{H}_{300}$) that agree to within 0.2 eV.

Our NC results for this system without employing the statistical model, i.e., wherein an electron is added or removed from the system, yield values of 4.0, 3.9, and 4.9 eV for $V^+/V^0/V^-$. The formation energy for the positively charged vacancy state is within ~ 0.1 eV of the neutral vacancy, which appears consistent with other GGA calculations. The formation energy for the negatively charged vacancy compared to the neutral vacancy energy is ~ 1 eV larger. This is higher than the statistical model value of ~ 0.6 eV. We note that the negatively charged value appears to decrease as a function of NC size. Some of the difference might be reduced if we considered an even larger NC.

As the size of the NC decreases, the vacancy formation energies increase, i.e., the energy required to introduce a vacancy in the NC becomes less favorable. This trend, as illustrated in Fig. 7, is not accessible within supercell geometries since the systems are not confined. Similar effects are known for other energetically unfavorable defects in NCs and results from a phenomena known as “self-purification” [88]. Within a NC an energetically unfavorable defect may readily diffuse to the surface and lower the energy of the system [88]. We know that the reconstruction energy of a vacancy is significant [78]. As the NC increases in size, the strain energy associated with the vacancy becomes dispersed across a large number of atoms and the vacancy formation energy is reduced. Small NCs exhibit a strong strain energy per atom since the strain is distributed only over the first couple of shells. For large NCs, the additional shells are not strongly perturbed. Also, quantum confinement is known to alter the electronic states for small NC’s, e.g., the band gap is known to increase as the size of the NC decreases. The role of quantum confinement in

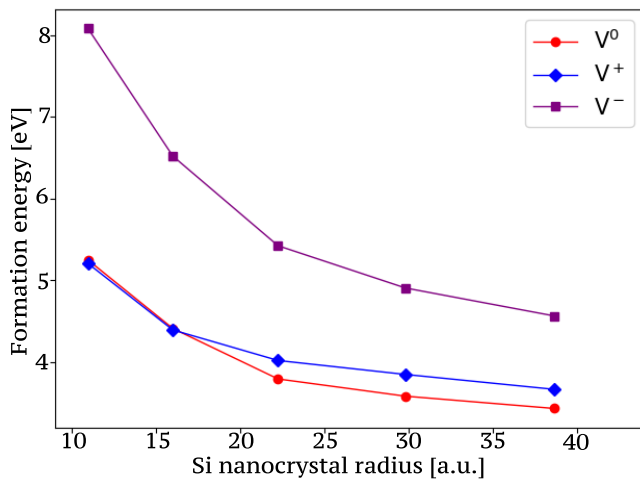


FIG. 7. Formation energies for neutral and charged vacancy.

terms of formation energies does not lend itself to a simple interpretation. The electronic states are physically confined for smaller NCs; however, defect states tend to be localized and are not as strongly affected by confinement. This accounts for the lack of a strong size dependence for the relative energy differences between the charged states.

The relative energy differences between adding and subtracting charge to the vacancies is clear from Fig. 6. For a positively charged vacancy V^+ , an electron is removed from the lowest gap state, leaving it half occupied. But when we add an electron, according to the V^- panel, we add it to a different state, a higher-energy state. In one case we are removing an electron from a filled state, and in the other case, we are adding an electron to an empty state.

V. SUMMARY

The ability to calculate dielectric and energetic properties of a large confined system allows us to consider charged

defects in bulk Si in a straightforward manner without invoking a supercell with a compensating background or the use of statistical models. The use of NCs for this purpose requires the use of large systems, typically composed of thousands of atoms. With the advent of real-space algorithms for solving the Kohn-Sham equations and the accompanying hardware, access to such NCs is feasible.

Here, we examined (i) the screening of a point charge and (ii) the formation of charged vacancies in hydrogen-terminated Si NCs. The screening function for our largest NC ($\text{Si}_{4403}\text{H}_{1060}$) has essentially converged to the bulk limit and is in agreement with a classical electrostatics model.

The formation energy for the neutral vacancy as determined from NC systems is consistent with the positron-lifetime experiments [33]. The point groups for the charged vacancies are also consistent with the electron paramagnetic resonance experiments and the well-known Watkins model [84].

Our work is consistent with calculations that use supercells with compensating backgrounds to handle Coulombic divergences. It is also consistent with calculations that invoke a statistical model where no compensating background is required. Moreover, unlike supercell computations, we can also investigate the role of quantum confinement for the vacancy formation energy as a function of the NC size. This reinforces the use of confined systems for modeling defects.

ACKNOWLEDGMENTS

We acknowledge support from a subaward from the Center for Computational Study of Excited-State Phenomena in Energy Materials at the Lawrence Berkeley National Laboratory, which is funded by the U.S. Department of Energy, Office of Science, Basic Energy Sciences, Materials Sciences and Engineering Division under Contract No. DEAC02-05CH11231, as part of the Computational Materials Sciences Program. High-performance computing resources were provided by the Texas Advanced Computing Center (TACC).

- [1] J. R. Chelikowsky and M. Ratner, Introduction: Nanoscience, nanotechnology and modeling, *Comput. Sci. Eng.* **3**, 40 (2001).
- [2] J. Chelikowsky, Why silicon is the benchmark, *Mater. Today* **5**, 64 (2002).
- [3] Y. Q. Wang, R. Smirani, and G. G. Ross, Stacking faults in Si nanocrystals, *Appl. Phys. Lett.* **86**, 221920 (2005).
- [4] J. Knipping, H. Wiggers, B. Rellinghaus, P. Roth, D. Konjhodzic, and C. Meier, Synthesis of high purity silicon nanoparticles in a low pressure microwave reactor, *J. Nanosci.* **4**, 1039 (2004).
- [5] L. Mangolini, E. Thimsen, and U. Kortshagen, High-yield plasma synthesis of luminescent silicon nanocrystals, *Nano Lett.* **5**, 655 (2005).
- [6] L. Mangolini, Synthesis, properties, and applications of silicon nanocrystals, *J. Vac. Sci. Technol. B* **31**, 020801 (2013).
- [7] A. D. Yoffe, Semiconductor quantum dots and related systems: Electronic, optical, luminescence and related properties of low dimensional systems, *Adv. Phys.* **50**, 1 (2001).
- [8] J. Liang, C. Huang, and X. Gong, Silicon nanocrystals and their composites: Syntheses, fluorescence mechanisms, and biological applications, *ACS Sustainable Chem. Eng.* **7**, 18213 (2019).
- [9] G. Hodes, When small is different: Some recent advances in concepts and applications of nanoscale phenomena, *Adv. Mater.* **19**, 639 (2007).
- [10] Y. Sun and J. Rogers, Inorganic semiconductors for flexible electronics, *Adv. Mater.* **19**, 1897 (2007).
- [11] S. T. Pantelides, The electronic structure of impurities and other point defects in semiconductors, *Rev. Mod. Phys.* **50**, 797 (1978).
- [12] L. Kronik, A. Makmal, M. L. Tiago, M. M. G. Alemany, M. Jain, X. Huang, Y. Saad, and J. R. Chelikowsky, PARSEC - the pseudopotential algorithm for real-space electronic structure calculations: Recent advances and novel applications to nanostructures, *Phys. Status Solidi B* **243**, 1063 (2006).
- [13] K.-H. Liou, C. Yang, and J. R. Chelikowsky, Scalable implementation of polynomial filtering for density functional theory

- calculation in PARSEC, *Comput. Phys. Commun.* **254**, 107330 (2020).
- [14] K. H. Liou, A. Biller, L. Kronik, and J. R. Chelikowsky, Space-filling curves for real-space electronic structure calculations, *J. Chem. Theory Comput.* **17**, 4039 (2021).
- [15] X. Cartoixa and L.-W. Wang, Microscopic Dielectric Response Functions in Semiconductor Quantum Dots, *Phys. Rev. Lett.* **94**, 236804 (2005).
- [16] C. Delerue, M. Lannoo, and G. Allan, Concept of dielectric constant for nanosized systems, *Phys. Rev. B* **68**, 115411 (2003).
- [17] F. Trani, D. Ninno, and G. Iadonisi, Tight-binding formulation of the dielectric response in semiconductor nanocrystals, *Phys. Rev. B* **76**, 085326 (2007).
- [18] D. Ninno, F. Trani, G. Cantele, K. J. Hameeuw, G. Iadonisi, E. Degoli, and S. Ossicini, Thomas-Fermi model of electronic screening in semiconductor nanocrystals, *Europhys. Lett.* **74**, 519 (2006).
- [19] S. Ögüt, R. Burdick, Y. Saad, and J. R. Chelikowsky, *Ab Initio* Calculations for Large Dielectric Matrices of Confined Systems, *Phys. Rev. Lett.* **90**, 127401 (2003).
- [20] M. Lannoo, C. Delerue, and G. Allan, Screening in Semiconductor Nanocrystallites and Its Consequences for Porous Silicon, *Phys. Rev. Lett.* **74**, 3415 (1995).
- [21] L.-W. Wang and A. Zunger, Dielectric Constants of Silicon Quantum Dots, *Phys. Rev. Lett.* **73**, 1039 (1994).
- [22] G. Allan, C. Delerue, M. Lannoo, and E. Martin, Hydrogenic impurity levels, dielectric constant, and Coulomb charging effects in silicon crystallites, *Phys. Rev. B* **52**, 11982 (1995).
- [23] F. Trani, D. Ninno, G. Cantele, G. Iadonisi, K. Hameeuw, E. Degoli, and S. Ossicini, Screening in semiconductor nanocrystals: *Ab initio* results and Thomas-Fermi theory, *Phys. Rev. B* **73**, 245430 (2006).
- [24] L.-W. Wang and X. Cartoixa, Motif-based polarization model: Calculations of the dielectric function and polarization in large nanostructures, *Phys. Rev. B* **75**, 205334 (2007).
- [25] A. Franceschetti and M. C. Tropicovsky, Screening of point charges in Si quantum dots, *Phys. Rev. B* **72**, 165311 (2005).
- [26] M. Leslie and N. J. Gillan, The energy and elastic dipole tensor of defects in ionic crystals calculated by the supercell method, *J. Phys. C* **18**, 973 (1985).
- [27] W. R. L. Lambrecht, Which electronic structure method for the study of defects: A commentary, *Phys. Status Solidi B* **248**, 1547 (2011).
- [28] S. B. Zhang and J. E. Northrup, Chemical Potential Dependence of Defect Formation Energies in GaAs: Application to Ga Self-Diffusion, *Phys. Rev. Lett.* **67**, 2339 (1991).
- [29] D. B. Laks, C. G. Van de Walle, G. F. Neumark, and S. T. Pantelides, Role of Native Defects in Wide-Band-Gap Semiconductors, *Phys. Rev. Lett.* **66**, 648 (1991).
- [30] D. B. Laks, C. G. Van de Walle, G. F. Neumark, P. E. Blöchl, and S. T. Pantelides, Native defects and self-compensation in ZnSe, *Phys. Rev. B* **45**, 10965 (1992).
- [31] Y.-N. Wu, X.-G. Zhang, and S. T. Pantelides, Fundamental Resolution of Difficulties in the Theory of Charged Point Defects in Semiconductors, *Phys. Rev. Lett.* **119**, 105501 (2017).
- [32] D. Maroudas and R. A. Brown, Calculation of thermodynamic and transport properties of intrinsic point defects in silicon, *Phys. Rev. B* **47**, 15562 (1993).
- [33] S. Dannefaer, P. Mascher, and D. Kerr, Monovacancy Formation Enthalpy in Silicon, *Phys. Rev. Lett.* **56**, 2195 (1986).
- [34] G. D. Watkins and J. W. Corbett, Defects in irradiated silicon: Electron paramagnetic resonance and electron-nuclear double resonance of the Si-*e* center, *Phys. Rev.* **134**, A1359 (1964).
- [35] Y. Shimizu, M. Uematsu, and K. M. Itoh, Experimental Evidence of the Vacancy-Mediated Silicon Self-Diffusion in Single-Crystalline Silicon, *Phys. Rev. Lett.* **98**, 095901 (2007).
- [36] N. Fukata, A. Kasuya, and M. Suezawa, Formation energy of vacancy in silicon determined by a new quenching method, *Phys. B: Condens. Matter* **308-310**, 1125 (2001).
- [37] H. Bracht, N. A. Stolwijk, and H. Mehrer, Properties of intrinsic point defects in silicon determined by zinc diffusion experiments under nonequilibrium conditions, *Phys. Rev. B* **52**, 16542 (1995).
- [38] H. Bracht, J. F. Pedersen, N. Zangenberg, A. N. Larsen, E. E. Haller, G. Lulli, and M. Posselt, Radiation Enhanced Silicon Self-Diffusion and the Silicon Vacancy at High Temperatures, *Phys. Rev. Lett.* **91**, 245502 (2003).
- [39] V. Ranki and K. Saarinen, Formation of Thermal Vacancies in Highly As and P Doped Si, *Phys. Rev. Lett.* **93**, 255502 (2004).
- [40] G. D. Watkins, The vacancy in silicon: Identical diffusion properties at cryogenic and elevated temperatures, *J. Appl. Phys.* **103**, 106106 (2008).
- [41] C. Freysoldt, B. Grabowski, T. Hickel, J. Neugebauer, G. Kresse, A. Janotti, and C. G. Van de Walle, First-principles calculations for point defects in solids, *Rev. Mod. Phys.* **86**, 253 (2014).
- [42] J.-H. Eom, T.-L. Chan, and J. R. Chelikowsky, Vacancies and B doping in Si nanocrystals, *Solid State Commun.* **150**, 130 (2010).
- [43] S. Beckman and J. R. Chelikowsky, The structure and properties of vacancies in Si nano-crystals calculated by real space pseudopotential methods, *Phys. B: Condens. Matter* **401-402**, 537 (2007).
- [44] S. Sholihun, M. Saito, T. Ohno, and T. Yamasaki, Density-functional-theory-based calculations of formation energy and concentration of the silicon monovacancy, *Jpn. J. Appl. Phys.* **54**, 041301 (2015).
- [45] H. Seong and L. J. Lewis, First-principles study of the structure and energetics of neutral divacancies in silicon, *Phys. Rev. B* **53**, 9791 (1996).
- [46] A. Antonelli, E. Kaxiras, and D. J. Chadi, Vacancy in Silicon Revisited: Structure and Pressure Effects, *Phys. Rev. Lett.* **81**, 2088 (1998).
- [47] J. A. Van Vechten, Divacancy binding enthalpy and contribution of divacancies to self-diffusion in Si, *Phys. Rev. B* **33**, 2674 (1986).
- [48] M. I. J. Probert and M. C. Payne, Improving the convergence of defect calculations in supercells: An *ab initio* study of the neutral silicon vacancy, *Phys. Rev. B* **67**, 075204 (2003).
- [49] O. K. Al-Mushadani and R. J. Needs, Free-energy calculations of intrinsic point defects in silicon, *Phys. Rev. B* **68**, 235205 (2003).
- [50] A. Zywiets, J. Furthmüller, and F. Bechstedt, Neutral vacancies in group-IV semiconductors, *Phys. Status Solidi B* **210**, 13 (1998).
- [51] F. Corsetti and A. A. Mostofi, System-size convergence of point defect properties: The case of the silicon vacancy, *Phys. Rev. B* **84**, 035209 (2011).
- [52] A. F. Wright, Density-functional-theory calculations for the silicon vacancy, *Phys. Rev. B* **74**, 165116 (2006).

- [53] M. J. Puska, S. Pöykkö, M. Pesola, and R. M. Nieminen, Convergence of supercell calculations for point defects in semiconductors: Vacancy in silicon, *Phys. Rev. B* **58**, 1318 (1998).
- [54] P. Śpiewak and K. J. Kurzydłowski, Formation and migration energies of the vacancy in Si calculated using the HSE06 range-separated hybrid functional, *Phys. Rev. B* **88**, 195204 (2013).
- [55] M. Ganchenkova, L. Oikkonen, V. Borodin, S. Nicolaysen, and R. Nieminen, Vacancies and E-centers in silicon as multi-symmetry defects, *Mater. Sci. Eng., B* **159-160**, 107 (2009).
- [56] P. A. Schultz, Theory of Defect Levels and the “Band Gap Problem” in Silicon, *Phys. Rev. Lett.* **96**, 246401 (2006).
- [57] J. Lento and R. M. Nieminen, Non-local screened-exchange calculations for defects in semiconductors: Vacancy in silicon, *J. Phys.: Condens. Matter* **15**, 4387 (2003).
- [58] Y. Bar-Yam and J. D. Joannopoulos, Electronic structure and total-energy migration barriers of silicon self-interstitials, *Phys. Rev. B* **30**, 1844 (1984).
- [59] C. A. Rozzi, D. Varsano, A. Marini, E. K. U. Gross, and A. Rubio, Exact Coulomb cutoff technique for supercell calculations, *Phys. Rev. B* **73**, 205119 (2006).
- [60] T.-L. Chan, A. J. Lee, and J. R. Chelikowsky, An effective capacitance model for computing the electronic properties of charged defects in crystals, *Comput. Phys. Commun.* **185**, 1564 (2014).
- [61] H.-P. Komsa, T. T. Rantala, and A. Pasquarello, Finite-size supercell correction schemes for charged defect calculations, *Phys. Rev. B* **86**, 045112 (2012).
- [62] K. Momma and F. Izumi, *VESTA3* for three-dimensional visualization of crystal, volumetric and morphology data, *J. Appl. Crystallogr.* **44**, 1272 (2011).
- [63] P. Hohenberg and W. Kohn, Inhomogeneous electron gas, *Phys. Rev.* **136**, B864 (1964).
- [64] W. Kohn and L. J. Sham, Self-consistent equations including exchange and correlation effects, *Phys. Rev.* **140**, A1133 (1965).
- [65] J. R. Chelikowsky, N. Troullier, and Y. Saad, Finite-Difference-Pseudopotential Method: Electronic Structure Calculations Without a Basis, *Phys. Rev. Lett.* **72**, 1240 (1994).
- [66] J. R. Chelikowsky, N. Troullier, K. Wu, and Y. Saad, Higher-order finite-difference pseudopotential method: An application to diatomic molecules, *Phys. Rev. B* **50**, 11355 (1994).
- [67] Details can be found at <http://real-space.org>.
- [68] D. M. Ceperley and B. J. Alder, Ground State of the Electron Gas by a Stochastic Method, *Phys. Rev. Lett.* **45**, 566 (1980).
- [69] J. P. Perdew and A. Zunger, Self-interaction correction to density-functional approximations for many-electron systems, *Phys. Rev. B* **23**, 5048 (1981).
- [70] N. Troullier and J. L. Martins, Efficient pseudopotentials for plane-wave calculations, *Phys. Rev. B* **43**, 1993 (1991).
- [71] R. H. Byrd, P. Lu, J. Nocedal, and C. Zhu, A limited memory algorithm for bound constrained optimization, *SIAM J. Sci. Comput.* **16**, 1190 (1995).
- [72] C. Zhu, R. H. Byrd, P. Lu, and J. Nocedal, Algorithm 778: L-BFGS-B: Fortran subroutines for large-scale bound-constrained optimization, *ACM Trans. Math. Softw.* **23**, 550 (1997).
- [73] J. L. Morales and J. Nocedal, Remark on “Algorithm 778: L-BFGS-B: Fortran subroutines for large-scale bound constrained optimization”, *ACM Trans. Math. Softw.* **38**, 1 (2011).
- [74] J. R. Chelikowsky, M. L. Tiago, Y. Saad, and Y. Zhou, Algorithms for the evolution of electronic properties in nanocrystals, *Comput. Phys. Commun.* **177**, 1 (2007).
- [75] R. Resta, Thomas-Fermi dielectric screening in semiconductors, *Phys. Rev. B* **16**, 2717 (1977).
- [76] We compute the chemical potential as the total energy per Si atom in the bulk using the same simulation parameters as the NC calculations. $\mu_{\text{Si}} = -108.18$ eV.
- [77] B. J. Abdullah, M. S. Omar, and Q. Jiang, Size dependence of the bulk modulus of Si nanocrystals, *Sādhanā* **43**, 174 (2018).
- [78] S. Ögüt, H. Kim, and J. R. Chelikowsky, *Ab initio* cluster calculations for vacancies in bulk Si, *Phys. Rev. B* **56**, R11353 (1997).
- [79] S. Ögüt and J. R. Chelikowsky, *Ab initio* investigation of point defects in bulk Si and Ge using a cluster method, *Phys. Rev. B* **64**, 245206 (2001).
- [80] A. Antonelli and J. Bernholc, Pressure effects on self-diffusion in silicon, *Phys. Rev. B* **40**, 10643 (1989).
- [81] C. Z. Wang, C. T. Chan, and K. M. Ho, Tight-Binding Molecular-Dynamics Study of Defects in Silicon, *Phys. Rev. Lett.* **66**, 189 (1991).
- [82] O. Sugino and A. Oshiyama, Vacancy in Si: Successful Description Within the Local-Density Approximation, *Phys. Rev. Lett.* **68**, 1858 (1992).
- [83] E. G. Song, E. Kim, Y. H. Lee, and Y. G. Hwang, Fully relaxed point defects in crystalline silicon, *Phys. Rev. B* **48**, 1486 (1993).
- [84] See G. D. Watkins, in *Deep Centers in Semiconductors*, edited by S. T. Pantelides (Gordon and Breach, New York, 1986), Chap. 3, and references therein for the Watkins linear-combination-of-atomic-orbitals model and a discussion of the results from experiments for vacancy in Si.
- [85] J. Bernholc, N. O. Lipari, and S. T. Pantelides, Self-Consistent Method for Point Defects in Semiconductors: Application to the Vacancy in Silicon, *Phys. Rev. Lett.* **41**, 895 (1978).
- [86] J. P. Perdew, K. Burke, and M. Ernzerhof, Generalized Gradient Approximation Made Simple, *Phys. Rev. Lett.* **77**, 3865 (1996).
- [87] J. P. Perdew, K. Burke, and M. Ernzerhof, Perdew, Burke, and Ernzerhof Reply, *Phys. Rev. Lett.* **80**, 891 (1998).
- [88] G. M. Dalpian and J. R. Chelikowsky, Self-Purification in Semiconductor Nanocrystals, *Phys. Rev. Lett.* **96**, 226802 (2006).